



**Slovak University of Technology in Bratislava
Faculty of Electrical Engineering and Information
Technology**

Ing. Luboš Podlucký

Dissertation Thesis Abstract

Progressive devices for integrated photonics

to obtain the Academic Title of Philosophiae doctor (PhD.)

the doctorate degree study programme: 2613V25 Electronics and Photonics
in the field of study: 2613 Electrotechnics
Form of Study: **full-time**

Bratislava 10.9.2021

Dissertation Thesis has been prepared at Institute of Electronics and Photonics, Faculty of Electrical Engineering and Information Technology, Slovak University of Technology in Bratislava.

Submitter: Ing. Ľuboš Podlucký
Institute of Electronics and Photonics
Faculty of Electrical Engineering and Information Technology
Slovak University of Technology in Bratislava
Ilkovičova 3, 81219 Bratislava

Supervisor: prof. Ing. František Uherek, PhD.
Institute of Electronics and Photonics
Faculty of Electrical Engineering and Information Technology
Slovak University of Technology in Bratislava
Ilkovičova 3, 81219 Bratislava

Readers: doc. Ing. Dušan Pudiš, PhD.
Department of Physics
Faculty of Electrical Engineering and Information Technology
University of Žilina
Univerzitná 1, 010 26 Žilina

doc. Ing. Vítěslav Jeřábek, PhD.
Department of Microelectronics
Faculty of Electrical Engineering
Czech Technical University in Prague
Technická 2, 166 27 Prague, Czech Republic

Dissertation Thesis Abstract was sent: 17.9.2021

Dissertation Thesis Defense will be held on at.....

at Faculty of Electrical Engineering and Information Technology
Slovak University of Technology in Bratislava
Ilkovičova 3, 81219 Bratislava

Prof. Dr. Ing. Miloš Oravec
Dean of FEEIT of STU
Ilkovičova 3, 81219 Bratislava

Contents

Introduction	4
Available platforms for photonic integrated circuits.....	5
Fabrication of SiON waveguides	9
Fabrication process	9
Deposition and annealing of SiON waveguide core film	10
Etching mask preparation and photolithography	11
Etching of SiON film.....	12
Deposition of SiO _x cladding film	12
Experimental results and discussion	13
Design and simulation	13
Design and simulation of SiON waveguides for visible light sensor systems	Chyba! Záložka nie je definovaná.
Design and simulation of SiON waveguides for communication applications	Chyba! Záložka nie je definovaná.
Mask design.....	Chyba! Záložka nie je definovaná.
Deposition, annealing, and characterization of SiON optical waveguide core film.....	16
Fabrication of a mask for ICP/RIE etching of SiON waveguides	23
ICP/RIE etching of SiON waveguide core film	24
Deposition and characterization of SiO _x passivation film	26
Verification of the fabricated SiON waveguide	27
Conclusion.....	29
Main gains of dissertation thesis related to defined objectives	31
References	32
Zoznam publikácií.....	35

Introduction

Microwave photonics (MWP), a field that uses optical devices and techniques to generate, process, control, and distribute high-speed radiofrequency (microwave) signals, has been at the center of interest of the research community for the past 30 years. Photonics for microwave engineering applications make the realization of high-performance ultra-broadband implementation of microwave signal generation, processing, and distribution possible, which is either too complex and costly or even not directly possible in the electric domain [1-3]. The main areas of use of the MWP are communication systems (cellular, wireless, and satellite), distributed antenna systems, cable television, optical signal processing, and the internet of things. These areas of use demand ever-increasing speed, bandwidth, and dynamic range. They also require small devices and exhibit large tunability and strong immunity to electromagnetic interference.

Numerous techniques have been proposed and demonstrated for generating and processing microwave signals, including generation of ultra-broadband signals, distribution, and transport of RF over fiber, wideband tunable filters, and photonics-enhanced radar system [1-3]. Nonetheless, these techniques were based on discrete optoelectronic components, standard optical fibers, and fiber-based components. Discrete optoelectronic components have a larger footprint, higher power consumption, and are costly. They also have issues with stability and flexibility.

Fortunately, Integrated Microwave Photonics (IMWP) addresses all these issues. IMWP combines MWP technology with photonic integration technologies [1-4]. As a result, it is possible to use photonics integration to obtain substantial footprint reduction of highly complex MWP systems, making them more comparable to RF circuits. Furthermore, photonic integration reduces coupling losses, cost, and power consumption. However, the main disadvantage of IMWP systems is scattering losses in optical waveguides and fiber-to-chip coupling, which were caused by light sources, modulators, and detectors located off-chip. Thus, integrated microwave photonics research concentrates on reducing on-chip losses, integrating as many components as possible on a single chip, and demonstrating device reconfiguration [4-6].

Available platforms for photonic integrated circuits

Major available platforms for photonic integrated circuits are compound semiconductors, mainly indium phosphide (InP), silicon-on-insulator (SOI), and dielectrics, mainly silicon nitride (Si_3N_4), silicon oxynitride (SiON). Each of these materials has its advantages and disadvantages; notwithstanding, particular functions have been shown in the past several years. The advantages and disadvantages of these platforms alongside hybrid integration and some new emerging platforms will be discussed in this section.

Indium Phosphide (InP)

InP is the only material that can monolithically integrate active and passive photonic components, including lasers, photodetectors, modulators, and optical amplifiers. InP also has a small bending radius in the order of 100 μm , which allows us to create very compact photonic circuits and is appealing for large-scale photonic integration. Multiple applications have been developed in InP photonics, e.g., optical beamforming, fully programmable microwave photonic filters using microring resonator (MRR) structures, and monolithic integrated optical phase-locked loop for coherent detection scheme. However, the main issue with InP photonics is their relatively high propagation loss, ranging from 1.5 to 3 dB/cm [7].

Silica PLCs

Silica glass planar lightwave circuits (PLCs) [1, 8, 9] are another platform used in integrated photonics. They have exceptional optical properties, such as low propagation loss. They can also be easily mass-produced. For example, the lowest propagation loss measured in Silica PLCs at $\lambda = 1550$ nm is 0.85 dB/cm, demonstrated using phosphorus-doped silica on a silicon waveguide. Nevertheless, this silica waveguide had a low refractive index contrast of a 0.7%, which is not ideal for photonic integration due to the high large bending radius of the waveguide, therefore a larger chip size [8, 9].

Multiple MWP applications have been demonstrated using Silica PLCs such as true time-delay beamforming network, wide-tuning-range optical delay line, arbitrary waveform generator (AWG), and integrated frequency discriminator. [8, 9].

Silicon-on-insulator (SOI)

Silicon photonics' most significant selling point is its compatibility with microelectronic Complementary Metal Oxide Semiconductor (CMOS) fabrication processes. This enables the co-integration of photonics and electronics and makes microwave photonic systems less costly and more compact. Silicon photonics has sizeable refractive index contrast between silicon ($n \approx 3.48$) and silica (SiO_2 , $n \approx 1.45$) which causes high optical confinement and allows to produce SOI with a relatively small bending radius (5 - 100 μm). Most advances in silicon photonics for MWP have focused on passive reconfigurable devices and devices exploiting optical nonlinearities. SOI waveguides exhibit an extensive range of propagation loss (0.1-3 dB/cm) based on the waveguide dimensions and processing conditions [10-12].

TriPleX

The TriPleX platform consists of waveguide geometries based on an alternating layer stack of two materials: Si_3N_4 and SiO_2 . The fabrication of SiO_2 and Si_3N_4 films is done using low-pressure chemical vapor deposition (LPCVD), which is CMOS compatible and enables low-cost volume production. All functionalities of the PIC-based on the TriPleX platform are constructed using standard basic building blocks, such as waveguides, splitters/combiners and couplers, spot-size converters, and phase tuning elements. The basic functionalities that have been realized are ring resonators, Mach-Zehnder interferometer filters, tunable delay lines, and waveguide switches. This platform is also used to fabricate integrated optical waveguides with an extremely low optical loss (less than 0.1 dB/cm) on silicon and glass substrates for all wavelengths between 405 nm and 2035 nm [1, 13, 14].

Silicon oxynitride

Silicon oxynitride (SiON) is an attractive candidate for a middle refractive index contrast integrated photonics core material. SiON waveguides with SiO_2 cladding have lower loss than other silicon-based waveguides [15-17].

SiON waveguides have substantially lower refractive index contrast, with SiON core having a refractive index in a range of $n \approx 1.45$ to ≈ 2.0 and cladding film with $n \approx 1.4$ than silicon waveguides (Si core has $n \approx 3.5$). Therefore, they exhibit lower optical loss, allowing much longer waveguides (delay lines). The propagation loss of SiON waveguides can be as low as 0.2 dB/cm or even lower [16]. By changing the oxygen and nitrogen ratios in the SiON waveguide, we can tune the refractive index in a range of $n \approx 1.45$ to ≈ 2.0 , which gives us significant design flexibility

suitable for different applications, e.g., filters, MRRs, dispersion compensators, and optical switches.

Hybrid integration platform

This platform combines different materials and utilizes their strengths to fabricate photonic integrated circuits. There are many different techniques for fabricating IMWP chips in this technology. These techniques include wafer-scale (heterogenous) integration techniques such as wafer bonding or direct epitaxial growth, mainly oriented for mass-produced applications, and chip-to-chip (hybrid) integration through vertical or edge coupling [18-20].

The most prominent area of heterogenous integration technology is the hybrid integration of III-V materials with silicon and silicon nitride [21-23]. This hybrid integration combines the ability of III-V semiconductor materials to produce reliable light sources and modulators with low-loss optical waveguides made from silicon nitride/ oxynitride.

Other platforms

Besides the major platforms discussed above, other platforms are considered for IMWP implementation, such as chalcogenide glasses [24-26], GaAs [27, 28], lithium niobate (LiNbO_3) [29, 30], polymers [31, 32], Ta_2O_5 [33, 34], and some 2D materials, such as graphene on SOI [35, 36]. These technologies are smaller in scale and volume, focusing on specific light-matter interactions, e.g., nonlinear optics, optomechanics, and plasmonics.

Objectives of the dissertation thesis

- Obtaining new knowledge in the preparation and characterization of SiON waveguide core film and SiO₂ passivation film for optical waveguides.
- Design and simulation of selected components utilizing SiON platform for communication applications and visible light sensor systems.
- Fabrication and verification of selected integrated photonics components utilizing SiON platform.

Fabrication of SiON waveguides

The SiON platform is suitable for implementing PICs with a middle refractive index contrast for the near-infrared and visible regions. Furthermore, like other Si-based technologies, SiON is CMOS compatible.

Additionally, it has lower refractive index contrast than other Si-based technologies, therefore lower propagation loss. SiON waveguides also have a core with a tunable refractive index ranging from 1.45 (SiO_2) to 2.0 (Si_3N_4). This incredible flexibility of refractive index selection increases the attractiveness of this material for the preparation of PICs for applications in information and communication systems and optical sensing. Furthermore, it allows the construction of planar waveguides with a favorable compromise between compactness, comparable dimensions to telecommunication optical fibers, and possible technological production processes [17].

Moreover, this technology is compatible with a very-large-scale integration (VLSI) technology. Therefore, it can be readily integrated with other silicon photonic devices in delay line-related applications, including phase array antennas and optical buffers used for optical networking. This technology is also compatible for hybrid integration with various older and newly emerging materials, e.g., III-V materials, BaTiO, VO_2 .

Fabrication process

The fabrication process of the SiON optical waveguides consists of multiple steps:

1. Deposition of the SiON optical waveguide core film
2. Annealing of the SiON film
3. Etching mask preparation and photolithography
4. Metal layer deposition
5. Lift-off process
6. Plasma etching of the SiON film
7. Wet etching of the remaining metal layer
8. Deposition of the SiO_x cladding film

The entire fabrication process of the SiON optical waveguide is shown in Fig. 1. Each step can be done using several technological processes.

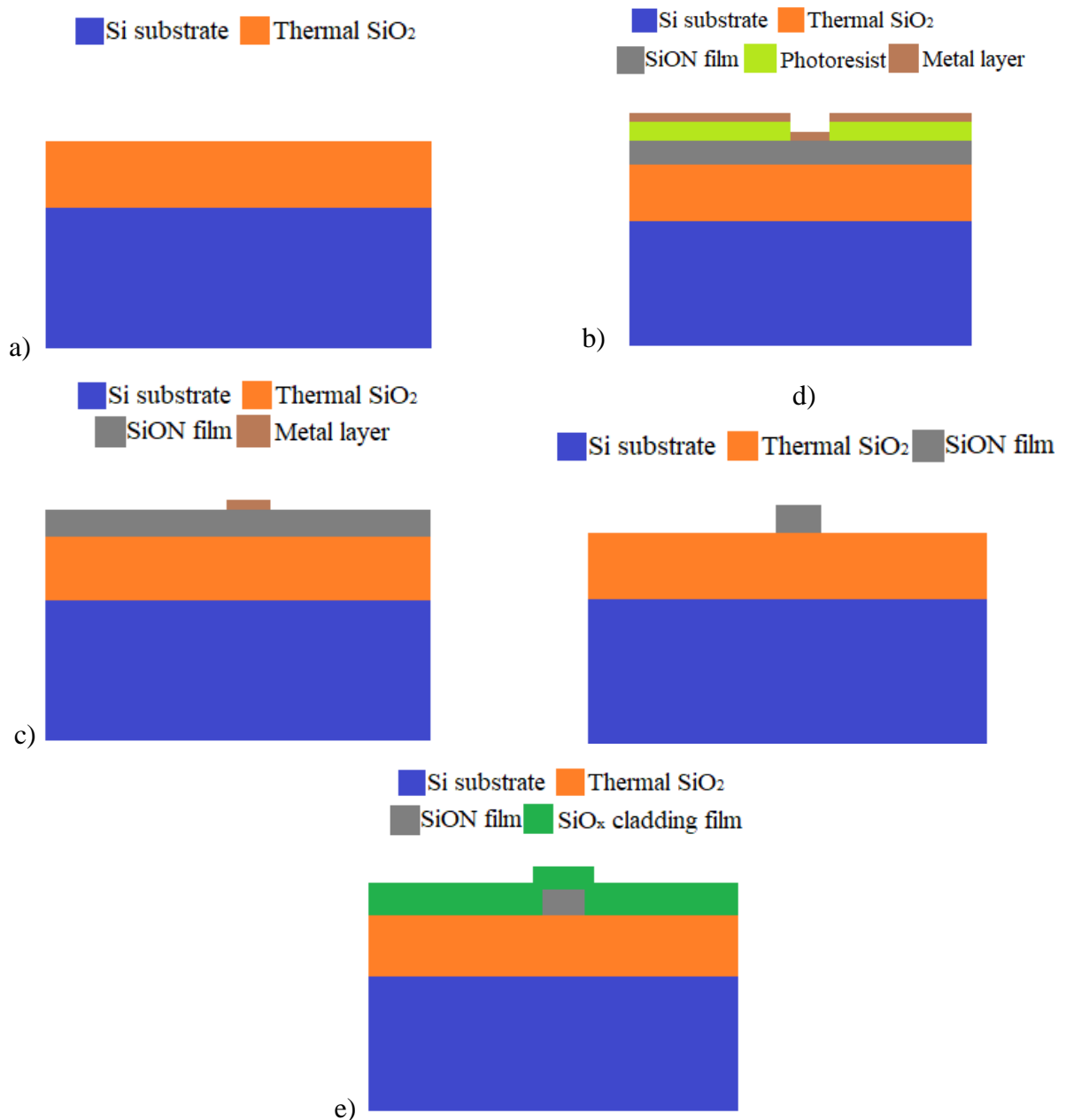


Fig. 1: a) Profile of Si wafer with 10 μm of thermal oxide, b) Model of the structure after SiON deposition, etching mask preparation, photolithography, and metal layer deposition, c) Model of the structure after the lift-off process, d) Model of the structure after plasma etching of SiON film and wet etching of the remaining metal mask, e) Model of the structure after the deposition of the SiO_x cladding film

Deposition and annealing of SiON waveguide core film

The deposition of SiON films can be done by several technological processes. The most common technological processes used for depositing films of optical waveguides are Low-Pressure Chemical Vapor Deposition (LPCVD) and Plasma Enhanced Chemical Vapor Deposition (PECVD). For the deposition of the SiON optical waveguide core film, PECVD technological process utilizing a parallel plate configuration reactor (Plasmalab 80+, Oxford Instruments, Abingdon, UK) was used.

In the PECVD process, deposition is done by introducing reactant gases between two parallel electrodes –an RF-energized electrode and a grounded electrode. The capacitive coupling between the electrodes excites the reactant gases into a plasma inducing a chemical reaction resulting in the deposition of the material on the substrate. The substrate placed on the grounded electrode is typically heated from 250°C to 350°C [37].

Standard reproducibility and uniformity of thickness of deposited SiON films by the PECVD process are between 1-3% [38]. The inhomogeneity and reproducibility of the refractive index are typically from 0.7 to 1.7% [38]. The gas mixture used for deposition of SiON film by the PECVD process contains silane (SiH₄) and ammonia (NH₃), which introduces unavoidable N – H, Si – H, and Si – O – H hydrogen bonds into the SiON film. This results in an absorption peak in a range of wavelengths from 1400 nm up to 1550 nm. This absorption impacts the overall performance of the optical circuit. By optimizing the technological fabrication processes of SiON films with high-temperature annealing, this absorption can be suppressed to an acceptable level below 0.2 dB/cm [38].

Etching mask preparation and photolithography

Photolithography is a process of transferring the pattern from the photomask into the photoresist to prepare the sample for subsequent processing, such as etching or deposition of additional material.

Etching mask material plays a substantial role in determining the morphology of the SiON waveguide core, such as sidewall smoothness, taper angle, and feature resolution. Therefore, choosing the suitable mask material for inductively coupled plasma /reactive ion etching (ICP/RIE) is crucial. One of the things poor etching masks can cause is rough or tapered sidewalls due to mask erosion.

One of the most popular materials for etching masks is a photoresist. The most significant advantage of a photoresist etching mask is that it is easy to fabricate, with no additional steps or processes. Nevertheless, the most known limitation of using a thick photoresist mask for high-resolution photolithography is pattern collapse caused by capillary force during rinsing liquid drying and after development. [39].

The most used approach to ICP/RIE etching with a huge substrate depth is to use a photoresist combined with an intermediate hard etching mask made of metal. The photoresist mask is first used to pattern and pattern transfer the intermediate metal hard mask using photolithography. Then the film is ICP/RIE etched using the patterned metal hard mask structure as an etching mask. The process for transferring the pattern into the metal is lift-off, which exposes

a pattern into the photoresist, depositing a thin metal film, then stripping away the remaining photoresist to leave behind the metal film only in the patterned area.

Etching of SiON film

The most common method for etching of the SiON film is dry etching, specifically ICP/RIE etching process. Various gases can be used for ICP/RIE etching, including sulfur hexafluoride (SF_6), hexafluoroethane (C_2F_6), and tetrafluoromethane (CF_4). The base of ICP/RIE etching is an inductively coupled plasma. The ICP source generates high-density plasma because of inductive coupling between the RF antenna and the plasma. The RF antenna generates an alternating RF magnetic field located in the plasma generation region. It induces an RF electric field, which then energizes electrons that participate in the ionization of gas molecules and atoms at low pressure. A low-pressure etching is advantageous for achieving a highly anisotropic profile and lowering contamination or damage to the substrate. In addition, no ion bombardment or erosion of the reactor walls occurs due to the absence of an electrical field near them [40].

Deposition of SiO_x cladding film

Multiple technical processes exist for the deposition of the SiO_x film. The most used methods are wet and dry thermal oxidation and PECVD [73]. Thermal oxidation produces higher quality oxide with lower surface roughness and stress, but the growth rate is very slow, making it impractical for thick oxide growth. On the other hand, the PECVD process for SiO_x deposition has a much higher growth rate, but the film's quality is lower [41]. Therefore, the PECVD process was used to deposit the SiO_x cladding film. The deposition of SiO_x cladding film works the same as the deposition of SiON waveguide core film. The gases used for the deposition of SiO_x cladding film are silane (SiH_4) and nitrous oxide (N_2O).

Experimental results and discussion

Design and simulation

The main objective of design and simulation is to find the physical dimensions of the strip optical waveguide and the optimum refractive index of the SiON optical waveguide core film for fabrication of the single-mode strip waveguide without the polarization mode dispersion. The design and simulation were done in the RSoft CAD Environment™ program and COMSOL Multiphysics® Version 5.6.

The dependency of n_{eff} of guided modes in a waveguide on the height of the waveguide was investigated for various waveguide thicknesses. The simulations were done for a specific wavelength of visible light $\lambda = 633\text{nm}$ in the RSoft CAD Environment™ program. The refractive indices of the core and the cladding of the waveguide were set to $n_1 = 1.46$ and $n_2 = 1.6$, respectively. The waveguide thicknesses ranged from $0.5\ \mu\text{m}$ up to $1\ \mu\text{m}$, with a step of $0.05\ \mu\text{m}$. Selected results of the simulations for waveguide thicknesses of $0.6\ \mu\text{m}$, $0.65\ \mu\text{m}$, and $0.7\ \mu\text{m}$ are shown in Fig. 2 a), b), and c), respectively.

From Fig. 2, it can be seen that the waveguide with any of the thicknesses used propagates the two fundamental modes' overall range of the simulated height of the waveguides. For the waveguide with a thickness of $0.6\ \mu\text{m}$, the other two modes will propagate from $0.7\ \mu\text{m}$ height and two more from $0.95\ \mu\text{m}$ height. For the waveguides with the thicknesses of $0.65\ \mu\text{m}$ and $0.7\ \mu\text{m}$, the other modes begin to propagate from $0.7\ \mu\text{m}$. It is also clear that the polarization mode dispersion (PMD) of the fundamental modes is zero for the waveguides that are square-shaped, i.e., their height and thickness are the exact sizes. Therefore, the waveguides that satisfy both conditions, i.e., they have zero PMD and are single-mode, are the ones shown in Fig. 2 a) and b).

Another set of simulations was done using COMSOL Multiphysics® Version 5.6 for the waveguides with dimensions of $0.6 \times 0.6\ \mu\text{m}^2$, $0.65 \times 0.65\ \mu\text{m}^2$, and $0.7 \times 0.7\ \mu\text{m}^2$. These simulations confirmed the results of the ones done in the RSoft CAD Environment™ program.

After examining the results of the simulations, the one chosen as the most suitable candidate for visible light sensor systems is a waveguide with the dimensions of $0.65 \times 0.65\ \mu\text{m}^2$, since they are the biggest dimension that satisfy both conditions.

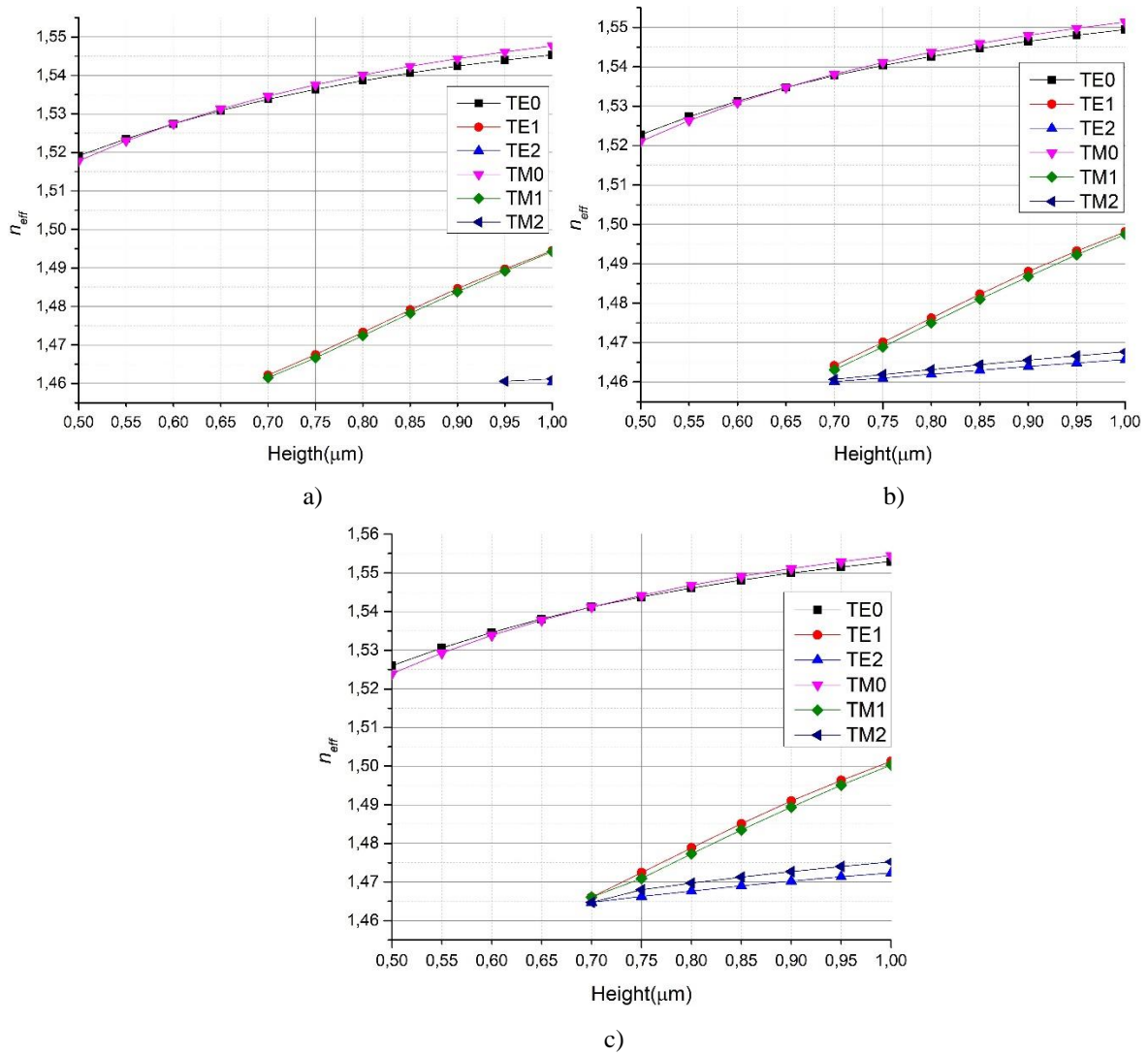


Fig. 2: The dependency of n_{eff} of guided modes in a waveguide on the height of the waveguide for waveguide thickness of a) 0.6 μm , b) 0.65 μm , and c) 0.7 μm

The design and simulation of SiON waveguides for communication applications were published in [42]. Simulations of the guided modes were done by the 2D finite difference method for TE and TM polarization of radiation and 1550 nm wavelength band in air [42]. The refractive index of the SiON core, the bottom thermal SiO₂ layer, and the PECVD SiO₂ top film were set to $n_1 = 1.6$, $n_2 = 1.456$, and $n_3 = 1.48$, respectively.

The dependencies of n_{eff} of guided modes in a waveguide with the thickness of 2.0 μm , 2.5 μm , and 3.0 μm on the waveguide width were investigated. The waveguide with a thickness of 2 μm leads only two fundamental modes overall simulated waveguide width range. However, for waveguides with a thickness of 2.5 μm and 3.0 μm , four higher modes begin to propagate from the 3.2 μm waveguide width.

The difference between n_{eff} of the TE fundamental mode and n_{eff} of the TM fundamental mode was also investigated to determine the waveguide width at which a zero-polarization mode

dispersion (PMD) of the simulated waveguides occurs. From the simulation, it can be determined that the zero value of PMD occurs not at the square shape of the waveguide but when the waveguide width is slightly smaller than its thickness. This is caused by the inequality of the refractive indices of the thermal SiO₂ bottom film and the PECVD SiO_x top film. The list of all waveguide widths for waveguides with a thickness of 2.0 μm, 2.5 μm, and 3.0 μm for which PMD is equal to zero is shown in Table 1 [42].

Table 1 Waveguide widths for different waveguide thicknesses for which PMD is equal to zero

Waveguide thickness	Waveguide width
2.0 μm	1.8 μm
2.5 μm	2.3 μm
3.0 μm	2.8 μm

After examining the results of the simulations, the one chosen as the most suitable candidate for the fabrication of SiON waveguides for communication applications is the dimensions of the thickness of 2.5 μm and width of 2.3 μm. These dimensions and the refractive index contrast were chosen because they are bigger, therefore, easier to fabricate [42].

The photolithography mask for the fabrication of SiON waveguides and other optical components is shown in Fig. 3. This mask was designed in the RSoft CAD Environment™ program. This is only a test mask for optimizing the fabrication process of the SiON waveguides and other optical components. It contains SiON waveguides with various components such as delay lines, Y Couplers, MZIs, and MMI couplers.

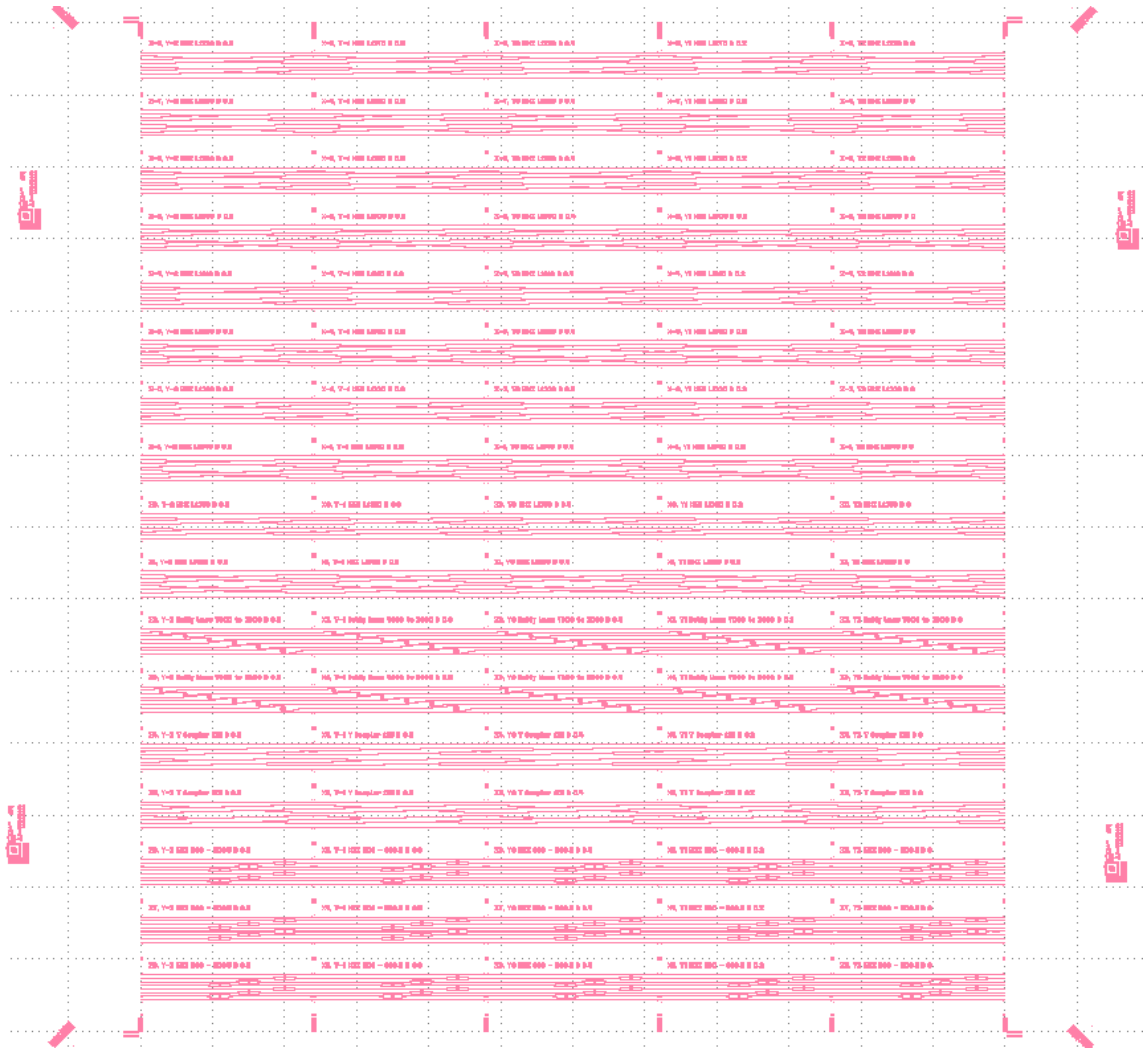


Fig. 3: Design of photolithography mask for fabrication of SiON waveguides and other optical components

Deposition, annealing, and characterization of SiON optical waveguide core film

The deposition of SiON films was done by the PECVD process utilizing a parallel plate configuration reactor (Plasmalab 80+, Oxford Instruments, Abingdon, UK). A standard 100 mm (4 in) polished Si wafers with (100) crystal orientation, the thickness of $525 \pm 20 \mu\text{m}$, and a 100 nm of thermal oxide on the surface were used as substrates for the fabrication of the SiON films.

Before the deposition, silicon wafers were cleaned in an ultrasonic bath with acetone, then cleaned in an ultrasonic bath with isopropyl alcohol, and then rinsed with demi water. The gas mixture for the deposition process contained silane (SiH_4)10%/Ar, nitrous oxide (N_2O), ammonia (NH_3), and N_2 . The deposition temperature was set to 300 °C, base pressure to 1 Torr, source power to 20 W, and the frequency of the PECVD reactor to 13.56 Mhz. The values of SiH_4 (10%)/Ar, NH_3 , and N_2 flow rates were 200, 20, and 600 sccm, respectively. In addition, the dependency of SiON film parameters on the N_2O flow rate was investigated [43].

SiO_x and SiN films were also deposited by the PECVD process as a comparison with the SiON films. A standard recipe was used for the deposition of the SiO_x film with the SiH₄ flow rate set to 85 sccm and an N₂O flow rate set to 710 sccm. The other parameters were the same as in the SiON film deposition. SiN film was deposited using a SiH₄ flow rate set to 200 sccm, an NH₃ flow rate set to 20 sccm, and an N₂ flow rate set to 300 sccm. The other parameters were the same as in the SiON film deposition [43].

The thickness, uniformity of thickness, and the refractive index of all samples were obtained with Micro-spot spectroscopic reflectometry (FilmTek 2000M, SCI, Carlsbad, CA, USA) and confirmed by spectroscopic ellipsometry (PhE-102, Angstrom Advanced Inc., Stoughton, MA, USA). The Cauchy model was used to calculate the refractive indices from both methods. The measured film thickness was used for the calculation of the deposition rates [43].

Fig. 4 a) shows the deposition rate (nm/min) of SiON film as a function of N₂O flow rate. It can be seen that the deposition rate of SiON films increases with increasing N₂O flow rate, which is caused by a higher oxygen amount in the plasma chamber [43].

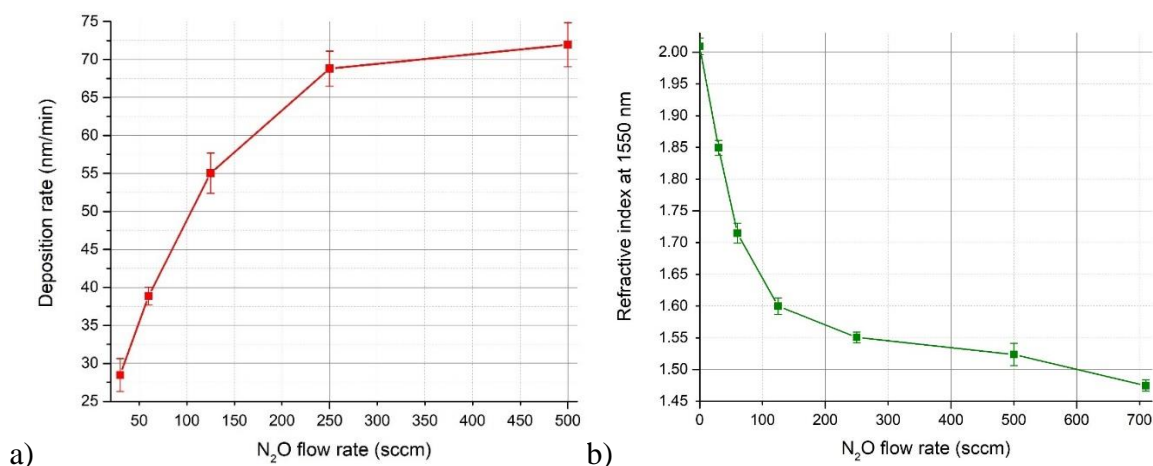


Fig. 4: a) Deposition rate (nm/min) of the SiON film deposited by the PECVD process as a function of N₂O flow rate, b) The refractive index of SiON, SiN, SiO_x films at wavelength $\lambda = 1550$ nm as a function of N₂O flow rate [43]

Fig. 4 b) shows the refractive index of SiON, SiN, and SiO_x films at $\lambda = 1550$ nm as a function of N₂O flow rate. It is clear that the refractive index decreases with increasing N₂O flow rate and has an exponential character. This decrease of refractive index can be explained by the fact that during the deposition of SiON films by the PECVD process, the most possible reaction is the formation of Si–O bonds. It is apparent that the refractive index closest to the target value of $n = 1.6$ is the refractive index of the SiON film deposited with N₂O flow rate = 120 sccm [43].

The refractive index of SiN, SiON, SiO_x films at wavelength $\lambda = 1550$ nm as a function of N₂O flow rate is shown in Fig. 5. Functions labeled as SION1-5 in Fig. 5 represent SiON films deposited with N₂O flow rates = 30, 60, 125, 250, and 500 sccm, respectively, shown in Table 5.2.

The values in the range from 1100 nm to 1600 nm were extrapolated from the measured data as the measuring equipment does not allow the measurement in this range of wavelengths. From the analysis of the reflectometry and ellipsometry measurements, it can be assumed that the N₂O flow rate can accurately control the refractive index of the deposited SiON films.

From the results of the reflectometry and ellipsometry measurements, the most suitable gas mixture for the fabrication of SiON films with the target value of refractive index $n = 1.6$ at $\lambda = 1550$ nm was the gas mixture of 200(SiH₄):20(NH₃):130(N₂O): 600(N₂) sccm [43].

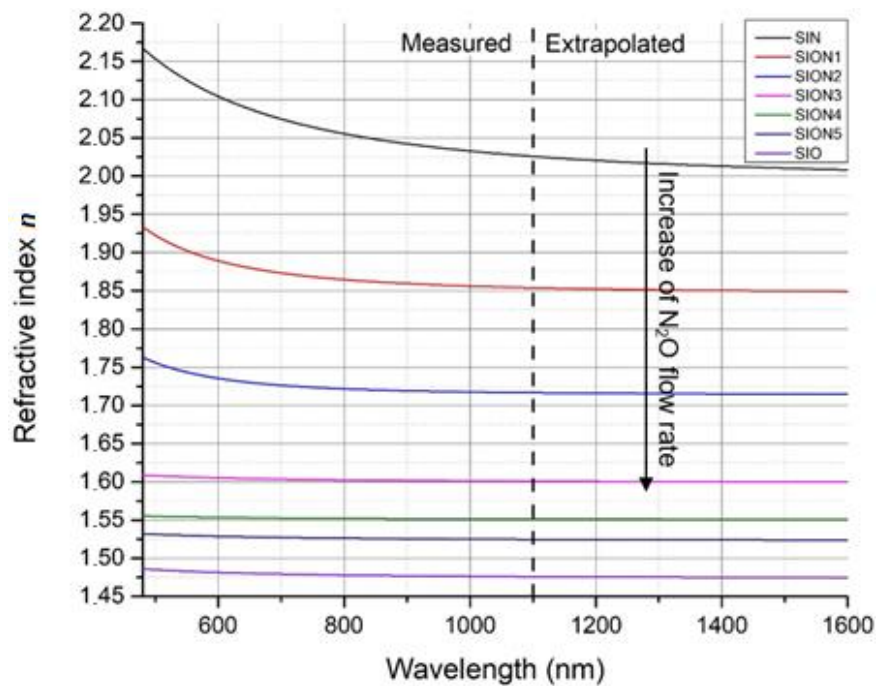


Fig. 5: Dependence of the refractive index for SiN, SiO_x, and SiON films on the wavelength [43]

The chemical composition of SiN, SiON, SiO_x films with a thickness of ≈ 500 nm was analyzed by Secondary Ion Mass Spectrometry (SIMS IV, Ion-TOF, Münster, Germany) with liquid metal ion gun Bi⁺ operated at 25 keV, and Cs⁺ ion sputtering operated at two keV in dual-beam mode. Fig. 6 shows the SIMS analysis of SiON film with an N₂O flow rate of 30 sccm. The exponential increase of the intensity of all elements in the SiON film is caused by the alteration of material conductivity with the measurement depth. From the analysis of all films, it is apparent that the concentration of oxygen-based elements (O⁻, O₂⁻, SiO⁻, SiO₂⁻) increases with increasing N₂O flow rate, and the concentration of nitrogen-based elements (SiN⁻, SiNO⁻ and SiNO₂⁻) decreases with increasing N₂O flow rate, as expected [43].

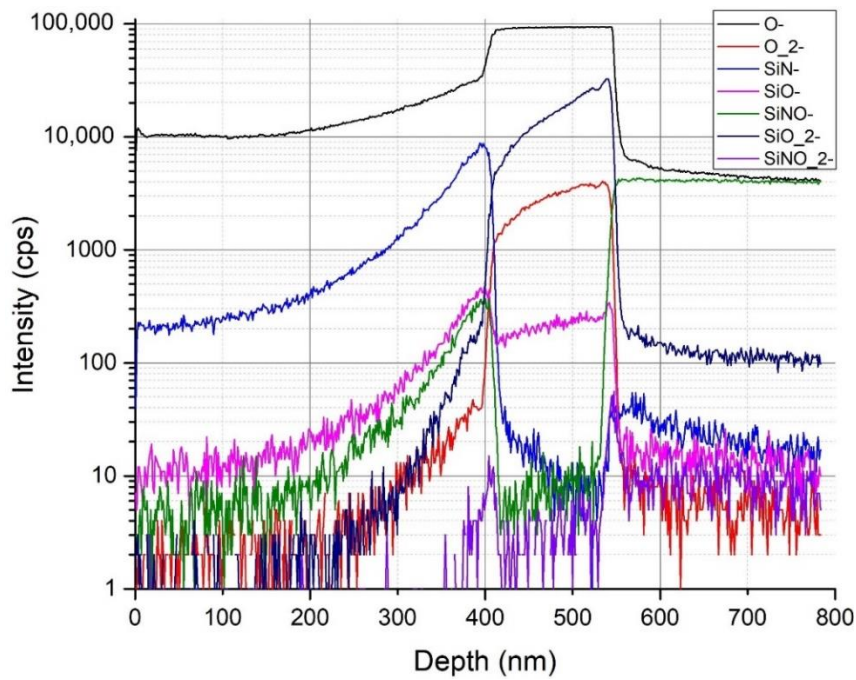


Fig. 6: SIMS analysis of the SiON film with an N₂O flow rate of 30 sccm [43]

The standard deposition of SiON films by the PECVD process introduces hydrogen (H) as a component from SiH₄ and NH₃ into the SiON film. The hydrogen concentration level is crucial from the absorption peak point of view at $\lambda = 1550$ nm. Thus, it would be helpful to estimate the hydrogen concentration level. One way of the hydrogen concentration estimation is to compare the relative hydrogen concentration regarding the N₂O flow rate. Fig. 7 a) shows the relative concentration of hydrogen as a function of the N₂O flow rate, where 100% intensity is measured at an N₂O flow rate of 0 sccm (Si₃N₄ sample). The relative hydrogen concentration is not linear and decreases with increasing N₂O flow rate, which is apparent since the overall concentration of gases that contain hydrogen (SiH₄, NH₃) decreases with increasing N₂O flow rate [43].

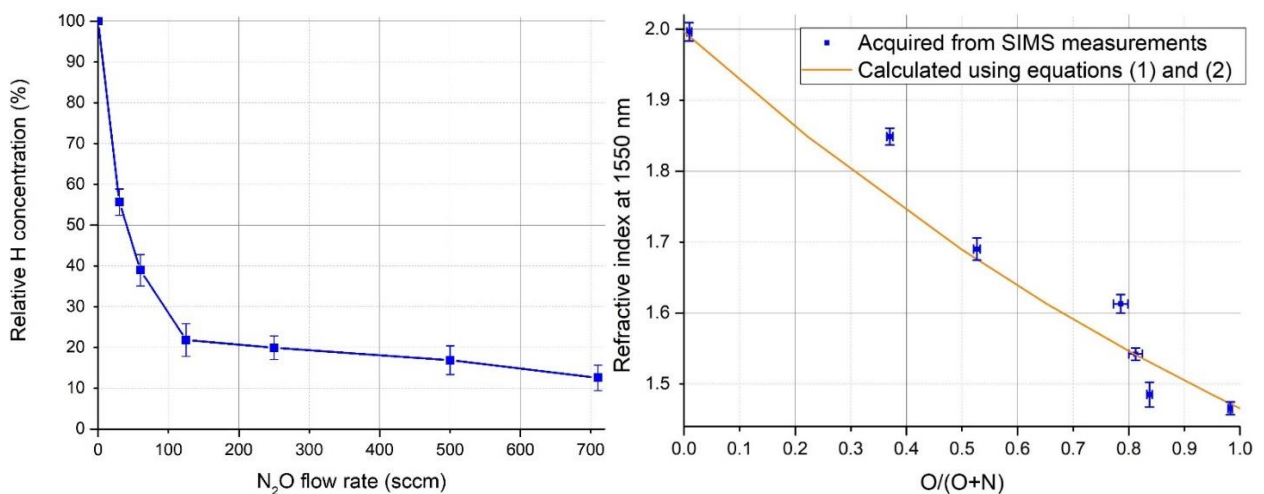


Fig. 7: a) Relative hydrogen (H) concentration as a function of N₂O flow rate, b) Refractive index at 1550 nm as a function of the O/(O + N) concentration ratio [43]

Fig. 7 b) shows the refractive index at $\lambda = 1550$ nm as a function of the O/(O + N) concentration ratio. The blue squares represent the data acquired from the SIMS measurements, and the line represents a refractive index calculation according to the Bruggeman effective medium approximation (EMA) method [43,44,45].

From Fig. 7 b), it is clear that the refractive index decreases with increasing oxygen concentration in the SiON film. Therefore, to gain more accurate results of the O/(O + N) concentration ratio acquired from SIMS measurements, a multiplication of $0.7 \cdot O$ was used as an ionization coefficient for oxygen.

The SiN, SiON, SiO_x films' surface roughness was analyzed using Atomic Force Microscopy (AFM, XE-100, Park Systems, Suwon, Korea) in tapping mode. The root mean square (RMS) surface roughness of the SiN, SiON, SiO_x films are shown in Table 2. It is clear that the N₂O flow rate does not affect the RMS surface roughness. Furthermore, even the highest measured RMS surface roughness should not introduce additional propagation losses into the SiON waveguides since it is much lower than half of the wavelength of the transmitted optical signal ($1550/1.6 = 969/2 = 484.5$ nm).

Table 2. RMS Surface roughness (nm) of SiN, SiO, SiON films [43]

Material film	N₂O flow rate (sccm)	RMS Surface roughness (nm)
SiN	0	50.95 ± 2.28
SiON1	30	70.24 ± 2.89
SiON2	60	16.33 ± 2.07
SiON3	125	59.77 ± 3.79
SiON4	250	36.53 ± 1.82
SiON5	500	54.55 ± 1.95
SiO ₂	710	33.68 ± 2.94

After the structural analysis of various SiON films, a 2500 nm thick SiON film was deposited on a standard 100 mm (4 in) polished Si wafer with (100) crystal orientation, a thickness of 525 ± 20 μ m, and 10 μ m of thermal oxide on the surface. The gas mixture for the fabrication of this SiON film was 200(SiH₄):20(NH₃):130(N₂O): 600(N₂) sccm, with the other parameters being the same as in the previous depositions [43].

The thickness, refractive index, and their uniformities of the SiON film were measured by Micro-spot spectroscopic reflectometry (FilmTek 2000M, SCI, Carlsbad, CA, USA). Nevertheless, the Cauchy model proved insufficient for the analysis because the difference

between the measured and simulated spectral reflectance was too significant. Thus, Scientific Computing International (SCI) model was used for the analysis.

Fig. 8 shows the AFM topography image of the analyzed SiON film with the image size of $10 \times 10 \mu\text{m}^2$. In order to highlight the surface roughness, the z -axis was magnified 20 times. As a result, the RMS surface roughness of the SiON film is approximately $5.32 \pm 0.46 \text{ nm}$. This roughness is much lower than the RMS surface roughness measured in the previous experiment, which is beneficial for the fabrication of SiON waveguides.

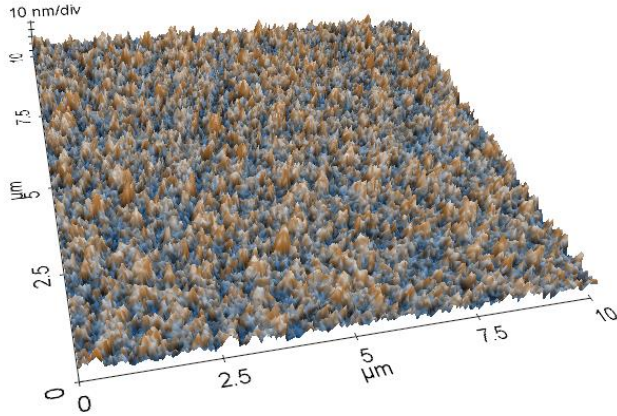


Fig. 8: Topography of $10 \times 10 \mu\text{m}^2$ image of a thick SiON film [43]

Fig. 9 shows the thickness and the uniformity of thickness of SiON film on the whole wafer. N represents the number of points measured on the wafer. From Fig. 9, it can be seen that the thickness of SiON film ranges from 2470 nm to 2522 nm, the uniformity of thickness is $\approx 1.05\%$, and the average thickness is $\approx 2505 \text{ nm}$, almost equal to the thickness goal of 2500 nm. It is clear that the thickness of the SiON film is highest in the center of the wafer and decreases from the center of the wafer to the edges [43].

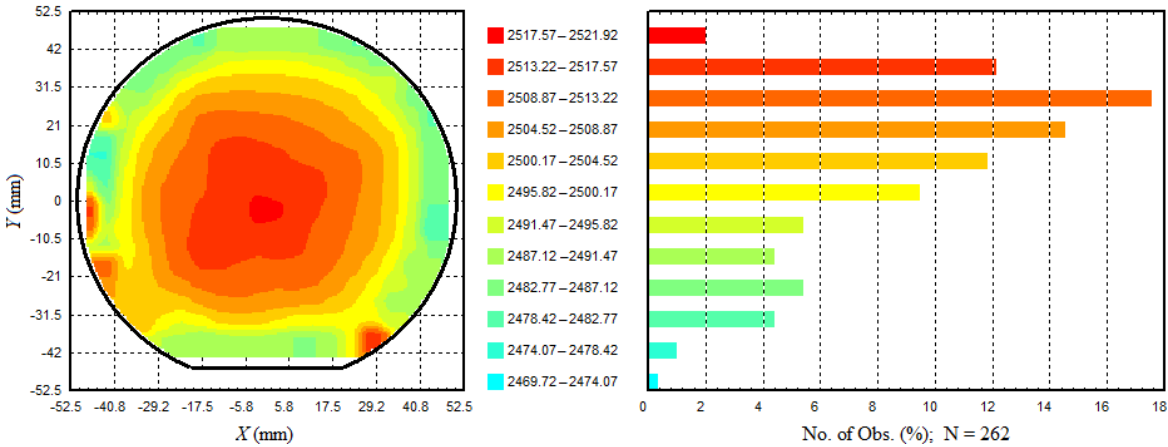


Fig. 9: Thickness and uniformity of thickness of a thick SiON film obtained by Micro-spot spectroscopic reflectometry, where N is the number of points measured on the wafer [43]

Fig. 10 shows the distribution of the refractive index of SiON film at $\lambda = 1550$ nm on the whole wafer. N represents the number of points measured on the wafer. The refractive index distribution is relatively even, with only the edges of the wafer having a refractive index slightly higher than the center of the wafer. The refractive index is in range from $n = 1.588$ to $n = 1.598$ with the average value of $n = 1.594$. This refractive index value is relatively close to the desired value of $n = 1.6$. The uniformity of the refractive index of the SiON film is 0.3%. The difference could be caused by the inaccuracies of the reflectometry measurement [43].

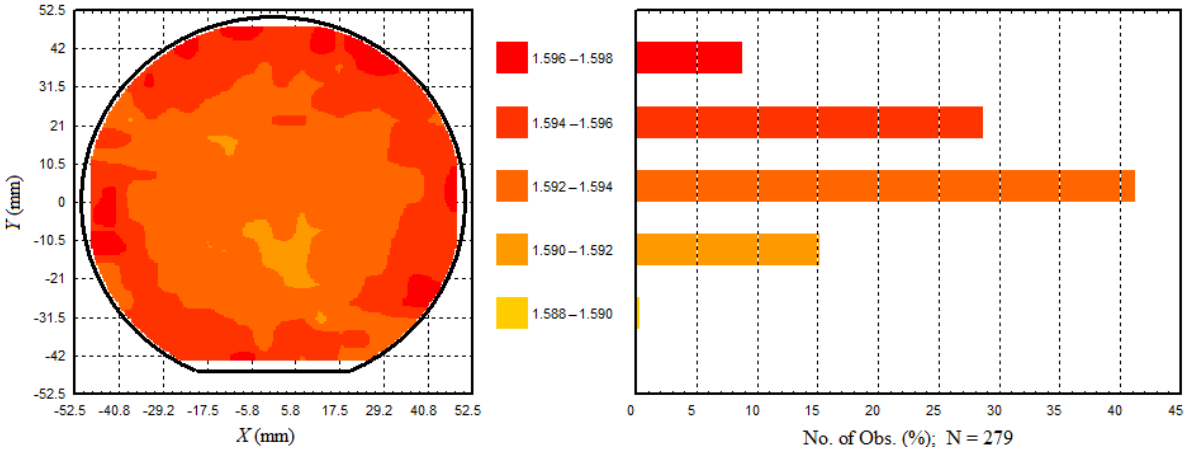


Fig. 10: Distribution of refractive index of a thick SiON film across a 100 mm wafer obtained by Micro-spot spectroscopic reflectometry [43]

After the deposition, the effect of annealing on the SiON film was investigated. The RTA was used to investigate the impact of temperature on reducing absorption peaks of hydrogen bonds. The temperatures and times used and the state of the SiON film after annealing are shown in Table 3. The SiON wafer was cut to 18 mm x 18 mm square samples for this experiment.

Table 3 Temperatures and Times of RTA

Temperature (°C)	Time (s)	State of the SiON film
700	15	Fractured
650	15	Fractured
600	15	Fractured
550	15	Fractured
500	15	Not fractured
500	20	Slightly fractured after two days
500	25	Fractured after two days
500	30	Fractured

The temperature of 500°C is too low, making RTA unusable for the annealing of the SiON films. Therefore, additional optimization of the SiON film annealing using the conventional annealing technique is required.

Mask fabrication for ICP/RIE etching of SiON waveguides

Two different masks were investigated: a very thick photoresist mask and a hard metal mask fabricated using a lift-off process.

Since the proposed waveguide structures are relatively large with a thickness of 2.5 μm and a width of 2.3 μm , a very thick photoresist mask is sufficient to fabricate the SiON waveguide core. However, the resolution of the very thick photoresist mask is not as good as the hard metal mask. ICP/RIE etching of SiON waveguide in an Oxford PlasmaLab 100 etching chamber using a very thick photoresist (thickness ~ 5000 nm) is shown in Fig. 11. The ICP/RIE etching parameters were $\text{CF}_4 = 50$ sccm, $\text{O}_2 = 0$ sccm, RIE = 200 W, $p = 50$ Torr, and $t = 30$ min. Due to, already mentioned, poor etching resistance, ICP plasma could not have been used, making the etching process much slower than the other two methods. Also, the resolution and the angle of sidewalls are very poor.

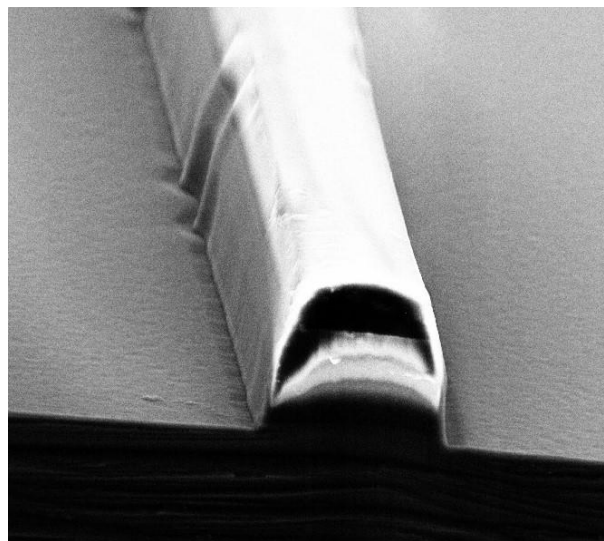


Fig. 11: ICP/RIE etching of SiON waveguide core film using a thick photoresist mask

The hard metal mask fabricated using the lift-off process yielded much better resolution than the thick photoresist mask. First, the SiON films were cleaned in acetone, isopropyl alcohol, and deionized water. Then the SiON film was coated with negative photoresist ma_N 1420 (micro resist technology GmbH, Berlin, Germany) and exposed with i-line filter photolithography in MA/BA 6 exposition chamber for 40 s. Then it was developed with MA-D 5335 Developer (micro

resist technology GmbH, Berlin, Germany) with two different development times: 60 s and 120 s, shown in Fig. 5.34 and 5.35, respectively.

After the photolithography process, the substrate was coated with 100 nm thick aluminum film using a thermal evaporation deposition platform (PRO Line PVD 75, Kurt J. Lesker Company, Jefferson Hills, PA, USA). Thermal evaporation was conducted at 10^{-6} Torr pressure with a deposition rate of 0.2 nm/s. The resist was then stripped with TechniStrip Micro D350, leaving the desired aluminum trace pattern for etching.

The aluminum waveguide pattern after the lift-off of photoresist with 120 s development time is shown in Fig. 12. It can be seen that the entire pattern has been correctly transferred from the photoresist to the aluminum with relatively smooth edges.

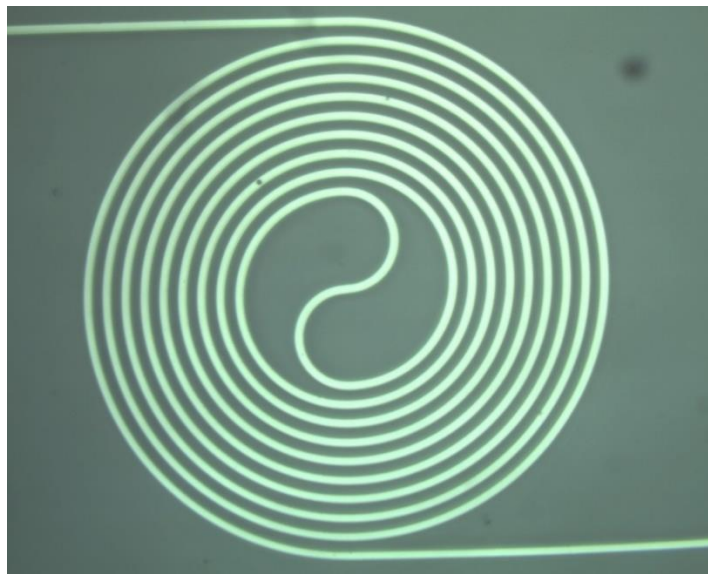


Fig. 12: Aluminum pattern of a delay line after the lift-off of the photoresist with 120 s development time

ICP/RIE etching optimization of SiON waveguide core film

SiON films were etched in an inductively coupled plasma reactive ion etching (ICP-RIE) chamber (Oxford Instruments Plasmalab 100, Abingdon, UK) using CF_4 gas. The impact of the oxygen (O_2) flow rate and source power (ICP) on etch rate and profile of SiON waveguides were investigated. In all cases, the flow rate of CF_4 , pressure, and bias power were set to 50 sccm, 5mTorr, and 50W, respectively. The flow rate of O_2 was set to 0, 2.5, and 5 sccm, and source power was set to 1000, 1200, and 1500 W for each O_2 flow rate, making it nine different samples. The etch time was set based on etch rate to remove the 2.5 μm thick SiON film from the uncovered surface. The profile angles were estimated with SEM (JSM-7500F, JEOL Ltd., Tokyo, Japan), and etch rate was estimated with a surface profilometer (DekTak 150, Veeco, Plainview, NY, USA). SEM images of etch profiles of all nine samples are shown in Fig. 13 [46].

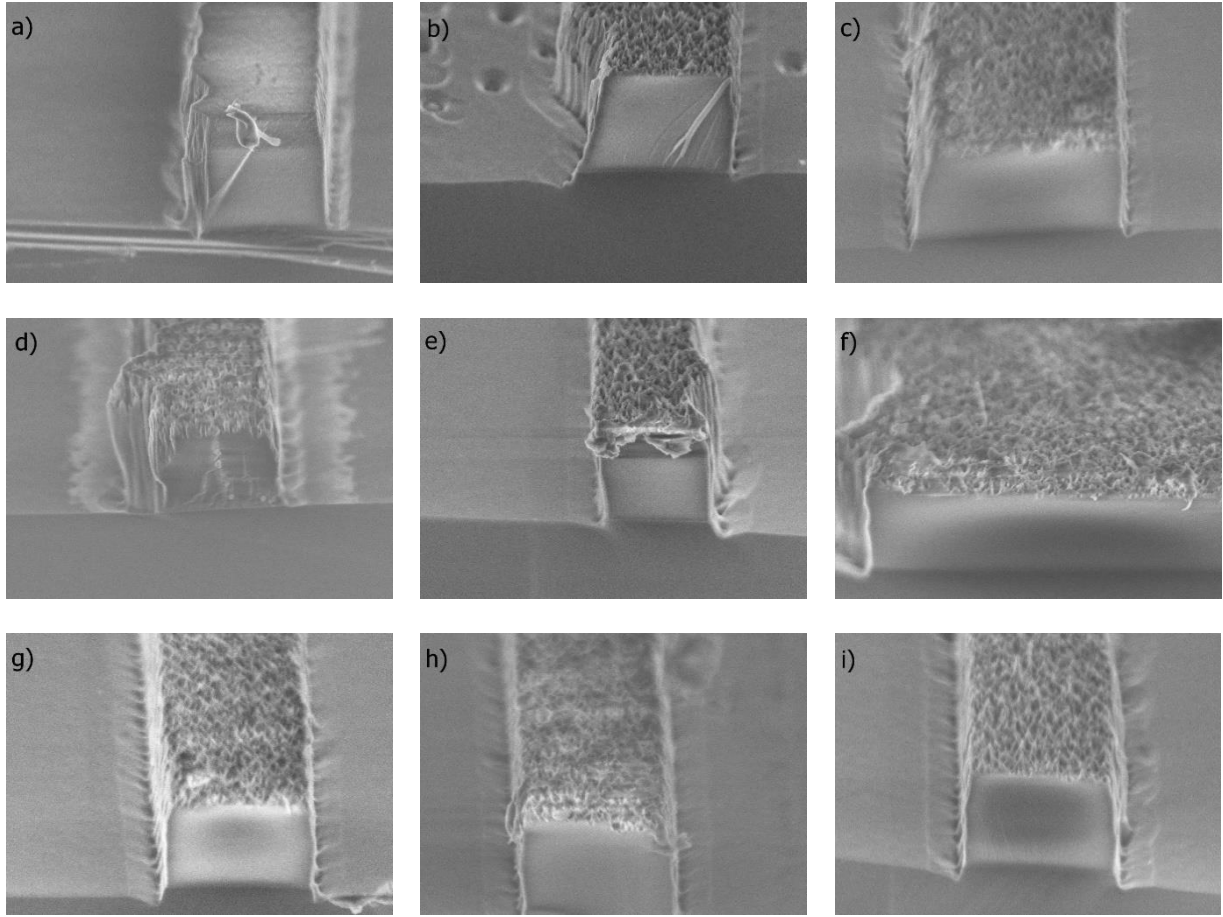


Fig. 13: SEM etch profiles obtained at: a) 1000W and 0sccm, b) 1000W and 2.5sccm, c) 1000W and 5sccm, d) 1200W and 0sccm, e) 1200W and 2.5sccm, f) 1200W and 5sccm, g) 1500W and 0sccm, h) 1500W and 2.5sccm, i) 1500W and 5sccm [46]

Table 4 shows etch rate and profile angle for various O₂ flow rates and source power combinations. As shown in Table 5.4, profile angles were similar in all cases in the range of 87 to 90°, unaffected by either source power or O₂ flow rate [81]. All these profile angles are satisfactory for the SiON waveguides and should not increase propagation losses in any way. As Table 4 shows, etch rate continuously increases with increasing source power due to enhanced plasma density but slightly decreases with increasing O₂ flow rate. This decrease can be explained by the fact that the SiON film already contained enough O₂, and adding additional O₂ lowered free fluorine (F) through gas-phase recombination [46].

After analyzing the ICP/RIE etching, the most suitable parameters selected for the etching of SiON waveguides were the CF₄ flow rate of 50 sccm, pressure 5 mTorr, bias power 50W, source power 1000 W, and O₂ flow rate 0 sccm.

Table 4 The effect of source power and O₂ flow rate on etch rate and profile angle [46]

source power (W)	O ₂ flow rate (sccm)	etch rate (nm/min)	profile angle (°)
1000	0	319	88
1000	2.5	297	90
1000	5	290	90
1200	0	365	88
1200	2.5	358	89
1200	5	345	90
1500	0	439	89
1500	2.5	426	90
1500	5	415	87

Deposition and characterization of SiO_x passivation film

SiO_x passivation film was deposited using the PECVD process in a parallel plate configuration reactor (Oxford PlasmaLab 80+, Oxford Instruments, Abingdon, UK). The precursor gas mixture contained SiH₄ (10% in Ar) and N₂O. The target thickness and refractive index were 5 μm and $n = 1.48$, respectively.

The impact of total gas flow rate, N₂O/SiH₄ ratio, and power on the refractive index, growth rate, and uniformity of the deposited SiO_x film thickness were investigated. The temperature and the pressure were set to 300°C and 1000 mTorr in all cases.

The values of the total flow rate, N₂O/SiH₄ ratio, and power P used are shown in Table 5. Table 5.5 also shows the deposition rate, uniformity of thickness, and refractive index of the SiO_x films. Refractive index, thickness, and uniformity were measured by Micro-spot Spectroscopic Reflectometry (FilmTek 2000M, SCI, Carlsbad, CA, USA). The average RMSE between calculated and measured reflectance for all samples was RMSE = 0.9783. The thickness of all samples was ≈5 μm.

From Table 5, it is possible to determine that the refractive index of the SiO₂ passivation film slightly decreases with increasing power. On the other hand, the deposition rate slightly increases with increasing power. This is because at higher power, the ionization of the gases during the deposition process is better, and the grown oxide does not have voids or particles [41]. Therefore, the refractive index value tends towards the one of thermal oxide as the power increases.

Table 5 Parameters used in SiO_x deposition and growth rate, uniformity of thickness, and refractive index of the SiO_x films

SiH ₄ (sccm)	N ₂ O (sccm)	N ₂ O/SiH ₄ ratio	Total Flow Rate (sccm)	P (W)	Deposition Rate (nm/min)	n	Uniformity (%)
85	710	8.353	795	20	64.74 ± 1.72	1.478 ± 0.006	0.90 ± 0.08
85	710	8.353	795	40	81.88 ± 3.25	1.476 ± 0.003	0.48 ± 0.13
85	710	8.353	795	100	84.59 ± 2.26	1.471 ± 0.005	0.55 ± 0.18
64	535	8.353	599	100	62.55 ± 1.03	1.485 ± 0.004	0.87 ± 0.10
108	900	8.353	1008	100	116.12 ± 4.17	1.464 ± 0.006	0.79 ± 0.15
62	740	12	802	100	62.55 ± 0.89	1.497 ± 0.005	0.67 ± 0.17
162	650	4	812	100	147.36 ± 5.08	1.458 ± 0.003	0.70 ± 0.16

The refractive index also decreases with increasing total flow rate, while the deposition rate increases with increasing total flow rate. This is explained by the fact that a lower total flow rate yields a dense SiO_x film due to a high transit time of the reactants during a deposition process, characterized by a higher refractive index, as explained by the Lorentz-Lorentz equation, which indicates that the refractive index increases with increasing density and vice-versa [41].

The deposition rate decreases with increasing N₂O/SiH₄ ratio because the quantity of Si ions decreases. The refractive index increases with increasing N₂O/SiH₄ ratio. This increase can be explained by the fact that at a high N₂O/SiH₄ ratio, more Si-O bonds are formed, while at a low N₂O/SiH₄ ratio, more Si-H bonds are formed [41].

From Table 5, it can be seen that the effect of power, total gas flow rate, and N₂O/SiH₄ ratio on uniformity of thickness of SiO_x passivation film is minimal, and the value of uniformity is under 1% for all samples. Therefore, after examining all analysis results, the parameters for deposition of SiO_x passivation film were chosen to be an N₂O/SiH₄ ratio of 8.353, a total gas flow rate of 795 sccm, and power $P = 20$ W.

Verification of the fabricated SiON waveguide

In order to verify the functionality of SiON waveguides, the wafer with fabricated structures had to be broken into smaller parts so that the wave can be guided into the tapers. One of the samples used to verify the functionality of SiON waveguides is shown in Fig. 14.

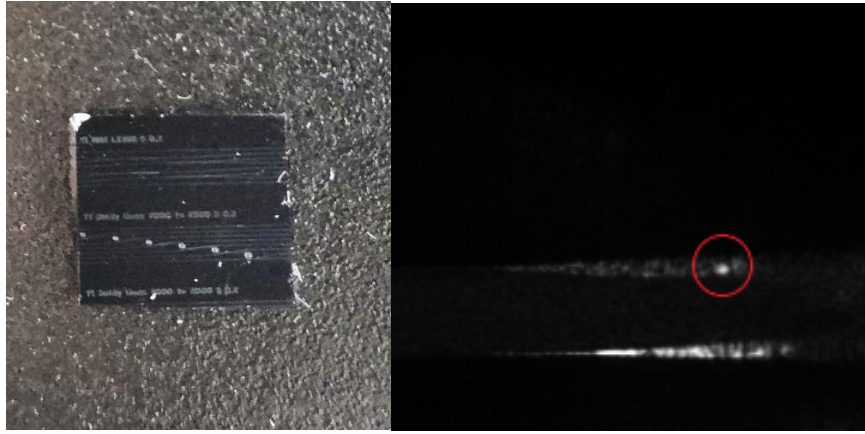


Fig. 14: a) Sample used for the verification of the functionality of SiON waveguides. b) The IR camera image of the light coming out of the SiON waveguide highlighted by a red circle

The verification process involved coupling a wave with a wavelength of 1550 nm into the taper of the SiON waveguide and capturing the wave coming out of the end of the waveguide using an IR camera (XEVA 320, Xenics nv, Leuven, Belgium). In order to couple the wave into the waveguide precisely, a fiber alignment machine (FL300, ficonTEC Service GmbH, Achim, Germany) was used. The optical fiber that guides the signal from the source to the SiON waveguide was single mode with a $9 \mu\text{m}^2$ diameter core.

The IR camera image of the wave coupled out of the SiON waveguide is shown in Fig. 14 b) demarcated by a red circle. By moving the input optical fiber by $2 \mu\text{m}$ to left or right, the light in the red circle diminished, and by moving it another $2 \mu\text{m}$, it disappeared, which confirms that it was, in fact, a waveguiding effect. An attempt to measure the output signal of the SiON waveguide was also made by removing the IR camera and aligning a second optical fiber, serving as a light sensor, with the output of the SiON waveguide. However, no signal was detected except noise.

Conclusion

The basic theory on MWP and IMWP, their advantages and drawbacks, and their applications in modern technology were studied in this work. In addition, the fabrication of optical waveguides and other optical components and complex structures in multiple material platforms was also studied. After extensive research into the material platforms for the fabrication of IMWP optical waveguides and other components, SiON was chosen as a suitable candidate for implementing photonic integrated circuits with a middle refractive index contrast for the visible and near-infrared region.

Simulations were done to find the physical dimensions of the strip optical waveguide and the optimum refractive index of the SiON optical waveguide core film for fabrication of the single-mode strip waveguide without the polarization mode dispersion. After examining the results of the simulations, a waveguide with a thickness of 2.5 μm and width of 2.3 μm was selected as the most suitable candidate for the fabrication of SiON waveguide for integrated optical communications and other optical components. The most suitable candidate for visible light sensor systems was a waveguide with the dimensions of 0.65x0.65 μm^2 , since this is the largest dimension that satisfies both conditions.

After the simulations, a photomask for fabrication was designed in the RSoft CAD Enviroment™ program. The photomask contained SiON waveguides with various components such as delay lines, Y Couplers, MZIs, and MMI couplers.

Subsequently, the fabrication process of SiON optical waveguides was investigated. Using technological processes at the Slovak University of Technology, each fabrication process step was characterized and optimized to achieve the parameters obtained by simulation.

SiON films were deposited by PECVD technological process. The dependency of various parameters, such as refractive index, deposition rate, surface roughness, chemical composition, on the N_2O gas flow rate was investigated. The gas mixture of 200:20:130:600 sccm (SiH_4 : NH_3 : N_2O : N_2) was deemed the best for the target value of the refractive index of the SiON film.

RTA was used to investigate the impact of temperature on reducing absorption peaks of hydrogen bonds of the SiON film. However, no experiments provided favorable results due to the high stress of the SiON film and further optimization is required.

Two different types of masks, a very thick photoresist mask and a hard metal mask fabricated using lift-off process, were investigated for ICP/RIE etching of SiON film. Aluminum hard mask fabricated using lift-off process has shown better resolution and fewer faults than the thick photoresist mask.

The impact of the oxygen (O_2) flow rate and source power (ICP) on etch rate and profile of SiON waveguides were also investigated. After a set of experiments, the SiON waveguide etched with the flow rate of O_2 set to 0 sccm and source power set to 1000 W was selected as the most suitable.

Finally, the impact of total gas flow rate, N_2O/SiH_4 ratio and power on the refractive index, growth rate, and uniformity of the SiO_x passivation film thickness was investigated. The SiO_x passivation film deposited with an N_2O/SiH_4 ratio of 8.353, the total gas flow rate of 1000 sccm, and power $P = 100$ W showed the most suitable refractive index.

Verification of fully fabricated SiON waveguides was done by coupling a wave into a taper of SiON waveguide and using an IR camera to capture the wave coupled out at the end of the waveguide. After comparing the image from the IR camera with the image of a 1:8 SiON splitter with $6 \times 6 \mu m^2$ dimensions commercially fabricated in China, it was concluded that the SiON waveguide does guide the wave with a wavelength of 1550 nm.

Main gains of dissertation thesis related to defined objectives

- New knowledge has been gained in the preparation of SiON waveguide core film and SiO₂ passivation film for optical waveguides utilizing the PECVD process.
- New knowledge has been gained in the characterization of SiON waveguide core film and SiO₂ passivation film for optical waveguides through the analysis of measured data obtained using various devices and techniques such as spectroscopic ellipsometry, micro-spot spectroscopic reflectometry, AFM, and SIMS.
- SiON waveguides were designed and simulated with specific dimensions and refractive index contrast to serve as single-mode waveguides with zero PMD at the wavelength of 1550 nm for communication applications.
- SiON waveguides were designed and simulated with specific dimensions and refractive index contrast to serve as single-mode waveguides at the wavelength of 632 nm for sensor systems.
- Optimization of the steps of the fabrication process of the SiON waveguides was achieved by analyzing the dependencies of the SiON waveguide properties on various processing parameters, such as N₂O flow rate during deposition, development time during etching mask preparation, or O₂ flow rate and source power during ICP/RIE etching.
- SiON waveguides for the waves of 1550 nm wavelength were fully fabricated and verified by coupling a wave into the taper of the SiON waveguide and using an IR camera to capture the wave coupled out of the waveguide exit.

References

- [1] Marpaung D.; Roeloffzen C.; Heideman R.; Leinse A.; Sales S.; Capmany J. Integrated microwave photonics, *Laser Photon. Rev.* 7, **2013**, 506–538.
- [2] Yao J. Microwave photonics, *J. Lightw. Technol.* 27, **2009**, 314–335.
- [3] Capmany J.; Novak, D. *Nat. Photonics* 1(6), 2007, 319–330.
- [4] Yi X.; Chew S.X.; Song S.; Nguyen L.; Minasian, R. Integrated Microwave Photonics for Wideband Signal Processing. *Photonics* **2017**, 4, 46.
- [5] Coldren L. in: Proceedings of the IEEE Topical Meeting on Microwave Photonics (MWP 2010), **2010**, Montreal, Canada.
- [6] Coldren L. et al. *Lightw. Technol.* 29(4), **2011**, 554 –570.
- [7] Fandiño J. S.; Muñoz P.; Doménech D.; Capmany J. A monolithic integrated photonic microwave filter, *Nat. Photonics* 11, **2016**, 124–129.
- [8] Horikawa K.; Ogawa I.; Kitoh T.; Ogawa H. in *Proceedings of the Optical Fiber Communications (OFC)*, **1996**, San Jose, CA, USA.
- [9] Himeno A.; Kato K.; Miya T. *IEEE J. Sel. Topics Quantum Electron*, **1998**, 4(6), 913 –924.
- [10] Xiao S.; Khan M. H.; Shen H.; Qi M. *Opt. Express* 15(22), **2007**, 14467–14475.
- [11] Rong H.; Xu S.; Kuo Y. H.; Sih V.; Cohen O.; Raday O.; Paniccia M. *Nat. Photonics*, **2007**, 1(4), 232–237.
- [12] Cardenas J.; Poitras C. B.; Robinson J. T.; Preston K.; Chen L.; Lipson M. *Opt. Express*, **2009**, 17(6), 4752–4757.
- [13] Heideman R.; Hoekman M.; Schreuder F. *IEEE J. Sel. Topics Quantum Electron*, **2012**, PP (99), 1.
- [14] Roeloffzen C. G. H. et al., Low-Loss Si₃N₄ TriPleX Optical Waveguides: Technology and Applications Overview, in *IEEE Journal of Selected Topics in Quantum Electronics*, **2018**, 24, 4, 1-21.
- [15] Melati D.; Morichetti F.; Melloni A. A unified approach for radiative losses and backscattering in optical waveguides, *IOP Publishing Ltd*, **2014**.
- [16] Bruno F.; del Giudice M.; Recca R.; Testa F. Plasma-enhanced chemical vapor deposition of low-loss SiON optical waveguides at 1.5- μ m wavelength; *Appl. Opt.* 30, **1991**, 4560-4564.
- [17] Yin L. et al., Fabrication and characterization of compact silicon oxynitride waveguides on silicon chips, *J. Opt.*, **2012**, 14 085501.
- [18] Morrison B. et al., Compact Brillouin devices through hybrid integration on silicon, *Optica* 4, **2017**, 847–854.
- [19] Komljenovic T. et al., Heterogeneous silicon photonic integrated circuits, *J. Lightw.*

Technol., **2016**, 34, 1, 20–35.

[20] Spencer D. T. et al. An optical-frequency synthesizer using integrated photonics, *Nature*, **2018**, 557, 81-85.

[21] He Y.; Lu Z.; Kuai X.; Feng Z.; Han W.; Li Z.; Yan W.; Yang F. Heterogeneous integration of InP and Si₃N₄ waveguides based on interlayer coupling for an integrated optical gyroscope, *Appl. Opt.*, **2021**, 60, 662-669.

[22] Soleimannezhad F.; Nikoufard M.; Mahdian MA. Low-loss indium phosphide-based hybrid plasmonic waveguide. *Microw Opt Technol Lett.*, **2020**, 1– 10.

[23] T. Hiraki et al., Membrane InGaAsP Mach–Zehnder Modulator Integrated With Optical Amplifier on Si Platform, *Journal of Lightwave Technology*, **2020**, 38, 11, 3030-3036.

[24] Zhou Y.; Lu R.; Wang G. et al., Graphene-Based Polarization-Independent Mid-Infrared Electro-Absorption Modulator Integrated in a Chalcogenide Glass Waveguide. *Nanoscale Res Lett.*, **2021**, 16, 80.

[25] Hwang J.; Kim D.; Han S.; Jeong D.; Lee Y.; Choi D.; Lee H. Supercontinuum generation in As₂S₃ waveguides fabricated without direct etching, *Opt. Lett.*, **2021**, 46, 2413-2416.

[26] Xia D. et al., On-Chip Broadband Mid-Infrared Supercontinuum Generation Based on Highly Nonlinear Chalcogenide Glass Waveguides, *Frontiers in Physics*, **2021**.

[27] Avrutin E.A.; Ryvkin B.S.; Kostamovaara J.T. AlGaAs/GaAs asymmetric-waveguide, short cavity laser diode design with a bulk active layer near the *p*-cladding for high pulsed power emission, *IET Optoelectronics*, **2021**.

[28] Wang Y.; Uppu R.; Zhou X.; Papon C.; Scholz S.; Wieck A.D.; Ludwig A.; Lodahl P.; Midolo L. Electroabsorption in gated GaAs nanophotonic waveguides, *Applied Physics Letters*, **2021**, 118, 131106.

[29] Yang J.; Wang C. Efficient terahertz generation scheme in a thin-film lithium niobate-silicon hybrid platform, *Opt. Express*, **2021**, 29, 16477-16486.

[30] Yang S.; Li Y.; Xu J.; M. Wang, Wu L.; Quan X.; Liu M.; Fu L.; Cheng X. Low loss ridge-waveguide grating couplers in lithium niobate on insulator, *Opt. Mater. Express*, **2021**, 11, 1366-1376.

[31] Kuang W.; Ma L.; Shi Y.; He Z. Ultra-Compact Low Loss Polymer Wavelength (De)Multiplexer with Spot-Size Convertor Using Topology Optimization, *IEEE Photonics Journal*, **2021**, 13, 3, 1-9.

[32] Zhang X. et al., Design of a Few-Mode Erbium-Ytterbium Co-Doped Polymer Optical Waveguide Amplifier With Low Differential Modal Gain, *Journal of Lightwave Technology*, **2021**, 39, 10, 3201-3216.

- [33] Fan R.; Lin YY.; Chang L. et al., Higher order mode supercontinuum generation in tantalum pentoxide (Ta₂O₅) channel waveguide, *Sci Rep* 11, **2021**, 7978.
- [34] Jung H.; Yu S.; Carlson D.; Drake T.; Briles T.; Papp S. Tantalum Kerr nonlinear integrated photonics, *Optica* 8, **2021**, 811-817.
- [35] Cui L.; Wang J.; Sun M. Graphene plasmon for optoelectronics, *Reviews in Physics*, **2021**, 6, 100054.
- [36] Heydari M.B.; Samiei M.H.V. Analytical Study of TM-Polarized Surface Plasmon Polaritons in Nonlinear Multi-Layer Graphene-Based Waveguides, *Plasmonics*, **2021**, 16, 841–848.
- [37] <http://www.plasma-therm.com/pecvd.html>
- [38] Worhoff K.; Lambeck P. V.; Driessen A. Design, Tolerance Analysis and Fabrication of Silicon Oxynitride Based Planar Optical Waveguides for Communication Devices, *Journal of Lightwave Technol.*, **1999**, 17(8), 1401- 1407.
- [39] Aydinoglu F.; Saffih F.; Dey R. K.; Cui B. Chromium oxide as a hard mask material better than metallic chromium, *Journal of Vacuum Science & Technology B*, **2017**.
- [40] Lita S.-R.; Wiesnoski A.; Zorich R. Advanced Semiconductor Fabrication Handbook, *Integrated circuit engineering Corp.*, **1998**. ISBN 10: 1877750700 ISBN 13: 9781877750700
- [41] Charavel R.; Olbrechts, B.; Raskin J.-P. Stress release of PECVD oxide by RTA, *Proc SPIE*, **2003**, 5116, 596-606.
- [42] Chovan J.; Figura D.; Chlpík J.; Lorenc D., Řeháček V.; Uherek F. Design, fabrication, and characterization of SiO_x/SiON/SiO₂/Si structures for passive optical waveguides realization, *Proceedings Volume 10603, Photonics, Devices, and Systems VII*, **2017**.
- [43] Podlucky L.; Vincze A.; Kováčová S.; Chlpík J.; Kováč J.; Uherek F. Optimization of Fabrication Process for SiON/SiO_x Films Applicable as Optical Waveguides, *Coatings* **2021**, 11, 574, ISSN 2079-6412.
- [44] Bruggeman D.A.G. Berechnung verschiedener physikalischer Konstanten von heterogenen Substanzen. I. Dielektrizitätskonstanten und Leitfähigkeiten der Mischkörper aus isotropen Substanzen. *Ann. Phys.* **1935**, 416, 636–664.
- [45] Kuiper A.E.T.; Koo S.W.; Habraken F.H.P.M. Deposition and composition of silicon oxynitride films. *J. Vac. Sci. Technol. B* **1983**, 1, 62–66.
- [46] Podlucky L.; Vojs M.; Chovan J.; Řeháček V.; Kováč J.; Uherek F. Optimization of SiON/SiO_x structures fabrication process for optical waveguides. *Radioelektronika* **2020**. Piscataway: IEEE, **2020**, 186-190.

Zoznam publikácií

ADC Vedecké práce v zahraničných karentovaných časopisoch

Počet záznamov: 1

Podlucký Ľ.; Vincze A.; Kováčová S.; Chlpík J.; Kováč J.; Uherek F. Optimization of Fabrication Process for SiON/SiO_x Films Applicable as Optical Waveguides, *Coatings* **2021**, *11*, 574 ISSN 2079-6412. [55%]

AFD Publikované príspevky na domácich vedeckých konferenciách

Počet záznamov: 5

Podlucký Ľ.; Vojs M.; Chovan J.; Řeháček V.; Kováč J.; Uherek F. Optimization of SiON/SiO_x structures fabrication process for optical waveguides. *Radioelektronika 2020*. Piscataway: IEEE, **2020**, 186-190, ISBN 978-1-7281-6468-7. [30%]

Podlucký Ľ.; Škriniarová J.; Kováč J.; Uherek F. Fabrication and characterization of ultra-thin dielectric films for plasmonics, *ADEPT 2020*, Žilina: Vydavateľstvo EDIS, **2020**, 78-81. ISBN 978-80-554-1735-6.

Chovan J.; Uherek F.; Haško D.; **Podlucký Ľ.**; Ziman M.; Koza E.; Pavlov J. Active alignment system of fiber array coupling to photonics integrated circuits, *ADEPT 2020*. Žilina: Vydavateľstvo EDIS, **2020**, 57-60. ISBN 978-80-554-1735-6.

Podlucký Ľ.; Uherek F.; Chovan J. Preparation of silicon photonics structures. *ELITECH'19*. Bratislava: Vydavateľstvo Spektrum STU, **2019**, ISBN 978-80-227-4915-2.

Podlucký Ľ.; Chovan J.; Figura D.; Uherek F.; Vojs M. SiON/SiO structures for photonic devices. *ADEPT 2019*. Žilina: University of Žilina, **2019**, 199-202. ISBN 978-80-554-1568-0.